DISCRETE AND CONTINUOUS
DYNAMICAL SYSTEMS SERIES B
Volume **19**, Number **5**, July **2014**

doi:10.3934/dcdsb.2014.19.1459

pp. **1459–1477**

GANG RIVALRY DYNAMICS VIA COUPLED POINT PROCESS NETWORKS

M. B. Short

School of Mathematics, Georgia Institute of Technology
Atlanta, GA 30332, USA

G. O. Mohler

Department of Mathematics and Computer Science, Santa Clara University
Santa Clara, CA 95053, USA

P. J. Brantingham

Department of Anthropology, UCLA
Los Angeles, CA 90095, USA

G. E. Tita

Department of Criminology, Law and Society, UC Irvine
Irvine, CA 92697, USA

Abstract. We introduce a point process model for inter-gang violence driven by retaliation – a core feature of gang behavior – and multi-party inhibition. Here, a coupled system of state-dependent jump stochastic differential equations is used to model the conditional intensities of the directed network of gang rivalries. The system admits an exact simulation strategy based upon Poisson thinning. The model produces a wide variety of transient or stationary weighted network configurations and we investigate under what conditions each type of network forms in the continuum limit. We then fit the model to gang violence data provided by the Hollenbeck district of the Los Angeles Police Department to measure the levels of excitation and inhibition present in gang violence dynamics, as well as the stability of gang rivalries in Hollenbeck.

1. **Introduction.** Gangs are defined by their willingness to use violence to further economic and social goals [15]. The economic goals of gangs may be related to the establishment and control of drug or other illicit markets [7, 30], but the social goals of gangs are equally, if not more important. Reputation is a primary currency of life on the street, and the problem of establishing, building, and maintaining reputation, or "street cred", is a core concern of gangs and gang members [1, 12, 23]. Violent attacks against rivals and violent responses to attacks by rivals offer an immediate remedy to the problem of establishing, building, and maintaining reputation.

That gangs and gang members generically seek reputation through violence does not necessarily specify the pattern of violence between gangs, though such patterning is readily apparent [6, 32, 23]. On the one hand, rival gangs appear to build up

2010 *Mathematics Subject Classification.* 60G55, 70K50, 91D99.

Key words and phrases. Stochastic dynamical systems, point processes, network dynamics, crime modeling.

This work was supported in part by AFOSR-MURI grant FA9550-10-1-0569, ARO grant 58344-MA, and NSF grant DMS-0968309.

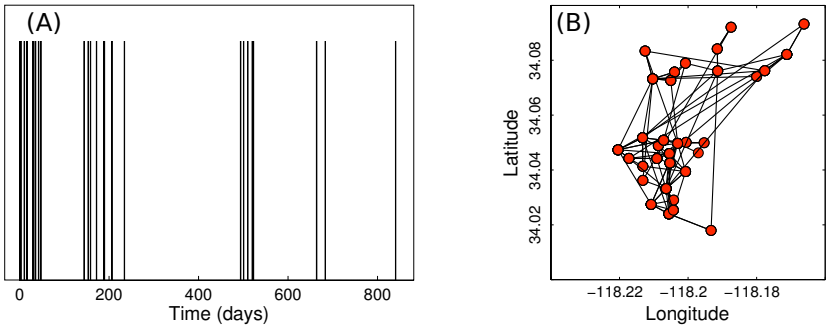

FIGURE 1. (A) Times of attacks between rival gangs Locke St. and Lowell St. occurring within the three year period 1999-2002. Note the clustered nature of the attacks. (B) Rivalry network of 33 gangs residing in or near Hollenbeck, Los Angeles during the same time period. The red dots denote gangs, placed at the mean geographic location where that gang was a victim of crimes. A link denotes at least one attack between a gang pair during the time interval.

enmity over relatively long periods of time, a form of long-lasting social memory not uncommon in tribal blood feuds [2]. On average, a gang is most likely to target their long-standing enemies over other gangs who are not seen as a threat. Geography appears to play an important role, with gangs based closer to one another in space more likely to express long-standing enmity [32, 31]. On the other hand, there is an immediacy to extreme violence that can override long-standing enmity. In general, crime provides immediate rewards (e.g., enhanced reputation) that offenders are often unwilling to pass up in favor of some uncertain and delayed payoff [9]. Thus, presented with an opportunity for immediate reputation gains via a violent act, gang members may opt to attack regardless of whether the target is a member of a long-standing rival or not. However, the salience of such rewards also appears to be time sensitive, adding to the inherent immediacy of violence. If a gang member does not respond quickly, and often with noticeable escalation, then the damage to individual and gang reputation may not be undone [12]. Allowing attacks to go unpunished has serious consequences on the street because word spreads rapidly that an individual or gang can be exploited with impunity.

Both long-standing enmity and situational factors contribute to the clustering of gang violence in space and time [31] (see Fig. 1). In the time dimension, which we focus on here, violence between rival gangs starts abruptly, but then forms dense groups of reprisals and counter reprisals, which end equally abruptly. We seek a model capable of capturing these dynamics not only between rival dyads, but also in environments consisting of multiple gangs. While studies conducted at the individual level have demonstrated the important role played by the presence of third parties [3, 24], we expand beyond dyads to examine how potential rivals, not directly involved in a given violent interaction, impact the stability of rivalry networks. We are also interested in how intervention in a rivalry impacts the stability of multi-gang networks and whether such interventions reduce the overall volume of crime.

1.1. **Background on crime modeling.** The behavioral basis of clustering in crime data has recently been investigated using reaction-diffusion PDEs [14, 26, 29, 33, 34], agent based models [6, 14, 33], and point processes [6, 18, 35]. A brief review of these models provides a foundation for understanding the clustering and dynamics of crime within a network of gangs. In the case of burglary, an initial crime has been shown to increase the likelihood of more crime at the same location, as well as neighboring houses within a few hundred meters [8, 13, 18, 35]. In [33], this phenomenon is modeled using the coupled PDE system,

$$\frac{\partial A}{\partial t} = \eta \nabla^2 A - A + A_0 + \rho A \ , \tag{1}$$

$$\frac{\partial \rho}{\partial t} = \vec{\nabla} \cdot \left[\vec{\nabla} \rho - \frac{2\rho}{A} \vec{\nabla} A \right] - \rho A + \overline{A} - A_0 \ , \tag{2}$$

where A denotes target attractiveness and ρ denotes criminal density. Here criminals diffuse in their urban environment, biased towards areas of high attractiveness. As they commit crimes, the local attractiveness is increased and macroscopic crime "hotspots" can form, where a majority of the total crime is localized in a few small areas. The stability of crime hotspots implies important consequences for policing strategies [14, 26, 34], as some hotspots can be suppressed while others can only be displaced.

In the context of gang violence, "hotspots" can form within the inter-gang rivalry network, localized within a small subset of the rivalry links between gangs [32]. In [6], temporal clustering in inter-gang violence data from the Hollenbeck district in Los Angeles is modeled using self-exciting point processes. In particular, a Hawkes Process with conditional intensity

$$\lambda(t) = \mu + \theta \sum_{t_i < t} \omega e^{-\omega(t - t_i)} \tag{3}$$

is used to model the increase in the rate of crime between gangs due to retaliation. Here, a fraction of crimes occur according to a Poisson process with intensity μ, representing attacks that occur by random chance. The overall rate of attacks λ is increased as each event t_i occurs, reflecting the propensity of gangs to respond to previous attacks. This leads to clusters of gang violence, with intermittent periods of inactivity due to the exponential decay of the second term in (3). Similar models taking the form

$$\lambda(t) = \mu + \sum_{t_i < t} g(t - t_i) \kappa(M_i)$$

are used to explain clustering patterns of earthquake aftershocks [19], where the increase in intensity depends on the magnitude, M_i, of each earthquake.

It is our goal here to capture excitation and inhibition in gang rivalry networks within the point process modeling framework. Excitation is expected to be primarily dyadic in nature; an attack by gang i on gang j increases the likelihood that j retaliates against i, not that j attacks a third gang k, or that a third gang k attacks i [22, 23]. Inhibition, by contrast, may arise in several ways not limited to interacting dyads. Inhibition might arise endogenously to the network. For example, if two gangs are focused on retaliating against each other, they may be significantly less likely to attack a third gang in the short term. Similarly, the ability of a particular gang to attack a rival may be suppressed through police intervention. In either case, inhibition of one gang may allow new rivalries to form among other gangs.

To capture these history-dependent relationships in gang rivalry networks, we propose a coupled system of state-dependent jump stochastic differential equations in Section 2. The solution to the system defines the conditional intensity of a marked point process, characterized by events between two gangs exciting that particular rivalry while inhibiting others. In Section 3, we outline an exact simulation strategy for the model. We then present numerical examples of the variety of transient and stationary rivalry networks that can form. In Section 4, we formulate a continuum description of the model and explain the variety of observed network topologies through analysis of this deterministic system. We then explore how the effectiveness of policing strategies may depend on network configuration in Section 5. Finally, in Section 6 we investigate the stability of gang rivalries in Los Angeles by fitting the model to gang violence data provided by the Hollenbeck district of the Los Angeles Police Department.

2. **Description of the model.** We consider a network of M gangs labeled by $i = 1, 2, ..., M$ and model the distribution of marked event times when gang i attacks gang j with a counting measure $N_{ij}(t)$. Letting t_{ij}^n denote the time of the n^{th} event where i attacks j, the counting measure can be interpreted through delta spikes located at the marked event times,

$$dN_{ij}(t) = \sum_{n=1}^{\infty} \delta(t - t_{ij}^n)dt \ , \tag{4}$$

or through its right continuous conditional intensity [4] $\lambda_{ij}(t)$, the rate of events when i attacks j (analogous to the rate of a Poisson process). The dependence on time reflects the fact that the intensity of the rivalry will be changing as events occur. We assume that the rivalry intensity can be written as a sum,

$$\lambda_{ij}(t) = \mu + g_{ij}(t) \ . \tag{5}$$

Here μ (independent of time) represents the baseline rate of attacks from gang i towards gang j. We assume that μ is the same for all gang dyads, which may be interpreted as each gang having long-standing rivalries of equal severity. More practically, μ reflects the stationary rate at which a rivalry produces violent events between any two gangs. The next term, $g_{ij}(t)$, represents the change in rivalry intensity due to past events where gang j has attacked gang i (excitation) or gang k has attacked gang i (inhibition). Thus $g_{ij}(t)$ may be interpreted as the situational rate of interactions that override long-standing rivalry characteristics.

To model the tendency of gangs to retaliate after an attack, we assume the intensity of gang i attacking gang j increases by an amount

$$f(\lambda_{ij}(t_-)) = \lim_{s \uparrow t} f(\lambda_{ij}(s))$$

(the limit as s approaches t from below, i.e., before the attack) following an attack by gang j against gang i at time t. The function $f(x)$ allows the response to attacks to depend on the current state of the system: for example, there may be a limit to the rate at which gangs attack due to finite resources, police presence, or other constraints on the system. For now, we consider the function $f(x) = \theta(1 - \nu x)$, where θ and ν are positive constants. We thus assume that the rivalry intensity jumps by a maximum of θ, and also that the intensity will never rise above a saturation point controlled by the parameter ν.

We also allow for the possibility of inhibition via third party rivalries so that, when gang k attacks gang i, we assume that the dynamic portion of the intensity g_{ij} for all $j \neq k$ decreases by a factor of $(1-\chi)$, where $\chi \leq 1$ is a parameter that controls the level of inhibition. In other words, the tendency of gang i to immediately retaliate against its most recent attacker, k, will divert i's attention away from rivalries with all other gangs j.

Finally, we assume that, in the absence of attacks, the rivalry intensity $\lambda_{ij}(t)$ decays back down to the baseline rate μ. The dynamic portion of the overall intensity then evolves according to the following nonlinear stochastic differential equation:

$$dg_{ij}(t) = -\omega g_{ij}(t)dt - \chi g_{ij}(t_-)\sum_{k\neq j,i} dN_{ki}(t) + f(\lambda_{ij}(t_-))dN_{ji}(t)\ . \tag{6}$$

We note that self-excitation and intra-gang violence [5] could also be added to Eq. (6). It is possible that after i attacks j, gang i may try to repeat a successful attack and thus $g_{ij}(t)$ may be forced by a term of the form $f_2(\lambda_{ij}(t_-))dN_{ij}(t)$. To include intra-gang violence, an equation for each diagonal term would be included,

$$dg_{ii}(t) = -\omega g_{ii}(t)dt - \chi g_{ii}(t_-)\sum_{k\neq i} dN_{ki}(t) + f_3(\lambda_{ii}(t_-))dN_{ii}(t)\ ,$$

and the sum in (6) would include $k = i$. Such a model would be useful in the context of data sets with both inter-gang and intra-gang crimes, but we will restrict our attention to Eq. (6) in the following sections.

3. **Simulation methodology and results.** The system of equations (6) can be sampled exactly, up to the error due to round-off and uniform random number generation. Because the intensity in (6) is non-increasing between events, Poisson thinning can be used to compute the event times [20]. Since the intensity decays exponentially between events, no numerical discretization is necessary. The overall simulation strategy is as follows. Given that the solutions $\lambda_{ij}(t)$ to (6) and event times $t^1, t^2, \ldots, t^n \leq s$ have been computed up to the current simulation time s:

1. Set $\beta = \sum_{i,j,i\neq j} \lambda_{ij}(s)$. This is simply the total rate of events at the current simulation time s.
2. Sample candidate event time $\tilde{t}$ according to a Poisson process with parameter β: $\tilde{t} = s - \log(u)/\beta$ where $u \sim U(0,1]$. This is the time at which the next event *may* occur.
3. Compute $g_{ij}(\tilde{t}_-) = g_{ij}(s)\exp[-\omega(\tilde{t}-s)]$ and $\lambda_{ij}(\tilde{t}_-) = \mu + g_{ij}(\tilde{t}_-)$, which are the excited and overall rates of the processes at candidate time $\tilde{t}$ (approached from the left), and $\tilde{\beta} = \sum_{i,j,i\neq j} \lambda_{ij}(\tilde{t}_-)$, the total rate of events at the candidate time (approached from the left). With probability $\tilde{\beta}/\beta \leq 1$, the candidate event is accepted as a true event, so that $t^{n+1} = \tilde{t}$, and we proceed to step 4. Otherwise, no event actually occurred, so we set the current simulation time $s = \tilde{t}$ and the current intensities $\lambda_{ij}(s) = \lambda_{ij}(\tilde{t}_-)$ and go to step 1.
4. Choose directed rivalry $l_1 \to l_2$ as the mark for event time $t^{n+1} = \tilde{t}$ with probability $\lambda_{l_1 l_2}(\tilde{t}_-)/\tilde{\beta}$. This tells us who ($l_1$) attacked whom ($l_2$) in this event.
5. Set current simulation time $s = \tilde{t}$ and update intensities via

$$\lambda_{ij}(s) = \lambda_{ij}(\tilde{t}_-) - \chi g_{ij}(\tilde{t}_-)1_{\{j\neq l_1, i=l_2\}} + f(\lambda_{ij}(\tilde{t}_-))1_{\{j=l_1,i=l_2\}}\ ,$$

where $1_{\{\}}$ denotes the indicator function. Go to step 1.

The solutions to the system (6) exhibit either transient or stationary networks depending on the parameter regime. Transient rivalry networks are characterized by either short bursts of events between gang dyads that quickly subside to be replaced by new rivalries (Fig. 2A), or by event clusters that are longer in duration and appear stable over intermediate timescales (Fig. 2B). As third party inhibition, χ, increases and ω and μ are decreased relative to θ, a phase transition occurs where stationary rivalries form between subsets of two or more gangs. For example, plotted in Fig. 2 are two possible stationary network configurations for 5 rival gangs. The first network (Fig. 2C) is characterized by three clear rivalry intensity levels: the highest occurs within each of two rivalry dyads (gangs 2 and 3, 4 and 5); the

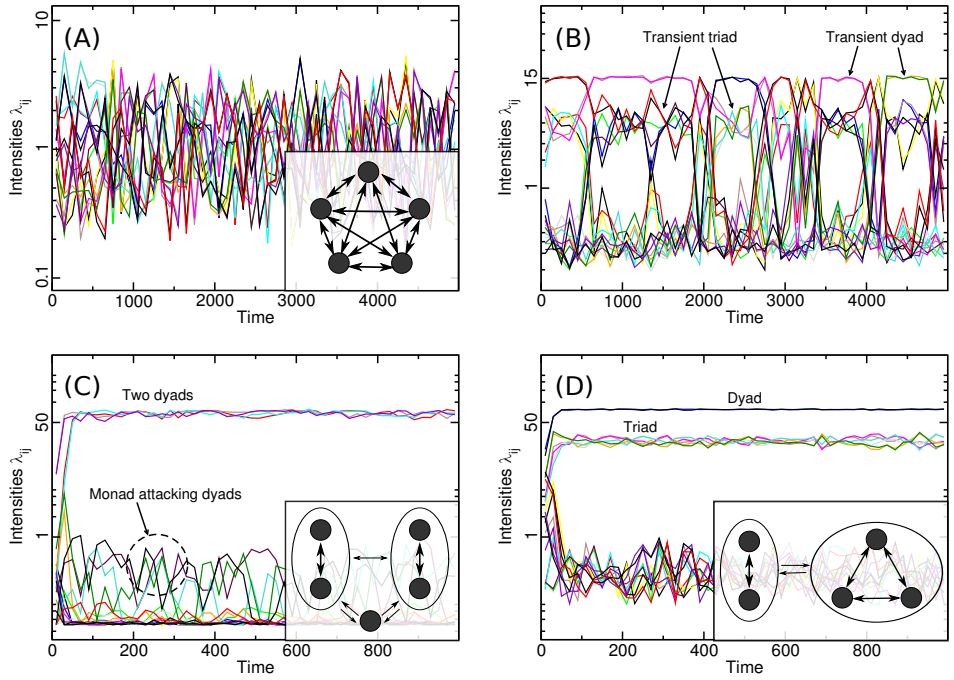

FIGURE 2. Rivalry intensities and network configurations for $M = 5$ gangs. (A) Fast timescale transient gang rivalries with $\mu = 0.1$, $\omega = 0.5$, $\chi = 0.1$, $\theta = 0.8$, $\nu = 0.05$. Here, all rivalries are essentially equal on average. (B) Intermediate timescale transient gang rivalries with $\mu = 0.1$, $\omega = 0.1$, $\chi = 0.1$, $\theta = 0.8$, $\nu = 0.05$. At any one time, the system typically presents one dyad and one triad, but the members of these groups change at random. (C) Stationary gang rivalries with $\mu = 0.05$, $\omega = 0.1$, $\chi = 0.15$, $\theta = 0.5$, $\nu = 0.01$ characterized by two gang rivalry dyads and a monad that attacks each of the other gangs at an intermediate intensity. Here, the monad attacks several times more than is attacked. (D) Stationary gang rivalries with $\mu = 0.1$, $\omega = 0.1$, $\chi = 0.01$, $\theta = 0.5$, $\nu = 0.01$ characterized by one rivalry dyad and one rivalry triad. In each simulation (A-D), the initial intensity of each rivalry is the baseline rate μ.

next highest corresponds to a monad (gang 1) attacking the members of the dyads (gangs 2 through 5); below this level are all other rivalries. The second network (Fig. 2D) is also characterized by three clear rivalry intensities, but they are different than those above: the highest corresponds to one rivalry dyad (gangs 1 and 2); the next highest between members of a rivalry triad (gangs 3 through 5); below this are rivalries between the dyad and triad. For certain parameter values, more than one equilibrium state is possible. For example, two triadic rivalries or three dyadic rivalries are possible network topologies in the case of a 6 gang network.

4. **Network classification.** To gain a better understanding of these phenomena, we consider a deterministic version of Eq. (6) in which events are no longer discrete, but happening continuously between gangs i and j at rate $\lambda_{ij}(t)$. The ODE we consider is therefore:

$$\frac{dg_{ij}}{dt} = -\omega g_{ij} - \chi g_{ij} \sum_{k\neq j,i} (g_{ki} + \mu) + \theta(1 - \nu g_{ij} - \nu\mu)(g_{ji} + \mu) \ .$$

Before working with this ODE, we express it in dimensionless form. Let dimensionless time $\tilde{t} = \omega t$ and dimensionless rivalry strength $\tilde{\lambda} = \tilde{g} + \tilde{\mu} = \nu g + \nu\mu$, and define $b = \theta/\omega$ and $a = \chi/\omega\nu$. In behavioral terms, b measures the strength of dyadic interactions while a measures the impact that third parties have on dyadic interactions. The equation then becomes, with tildes now dropped,

$$\frac{dg_{ij}}{dt} = -g_{ij} - a g_{ij} \sum_{k\neq j,i}^{M} (g_{ki} + \mu) + b(1 - g_{ij} - \mu)(g_{ji} + \mu) \ . \tag{7}$$

We restrict our further analysis to the case in which dimensionless $\mu < 1$, so that the time derivatives of the rivalry strengths can potentially be positive. In Fig. 3, we display simulation results for the system (7) using parameters that are equivalent to those of Fig. 2, noting that the ODE results closely match the average behavior of the stochastic system.

Given the system (7), we first find the fully symmetric, homogeneous equilibrium solution $g_{ij} = \overline{g}\ \forall i, j$, which may be interpreted as a complete graph with all rivalry ties of equal weight. This is found to be

$$\overline{g} = \Big[(b-1) - \mu\left[2b + a(M-2)\right] + \sqrt{\left((b-1) - \mu\left[2b + a(M-2)\right]\right)^2 + 4\mu b(1-\mu)\left[b + a(M-2)\right]}\Big] \Big/ 2\left[b + a(M-2)\right] \ . \tag{8}$$

In the special case $\mu = 0$, the homogeneous steady state $g_{ij} = 0\ \forall i, j$ is also a possible solution, as will be discussed in more detail below.

The stability of the homogeneous steady state depends on the parameters a, b, and μ, as well as on the total number of gangs M. For the case $M = 2$, the $\overline{g}$ state is always stable, and is in fact the only steady state solution to system (7) if $\mu > 0$. For $M > 2$, we find upon linearization of the system about the $\overline{g}$ state that there are a small number of unique eigenvalues: four of them if $M = 3$ and five if $M > 3$. The four eigenvalues that are shared between the $M = 3$ and $M > 3$ cases are

$$\lambda_1 = -d - q - u \ , \tag{9}$$

$$\lambda_2 = -d - (M-2)q + u \ , \tag{10}$$

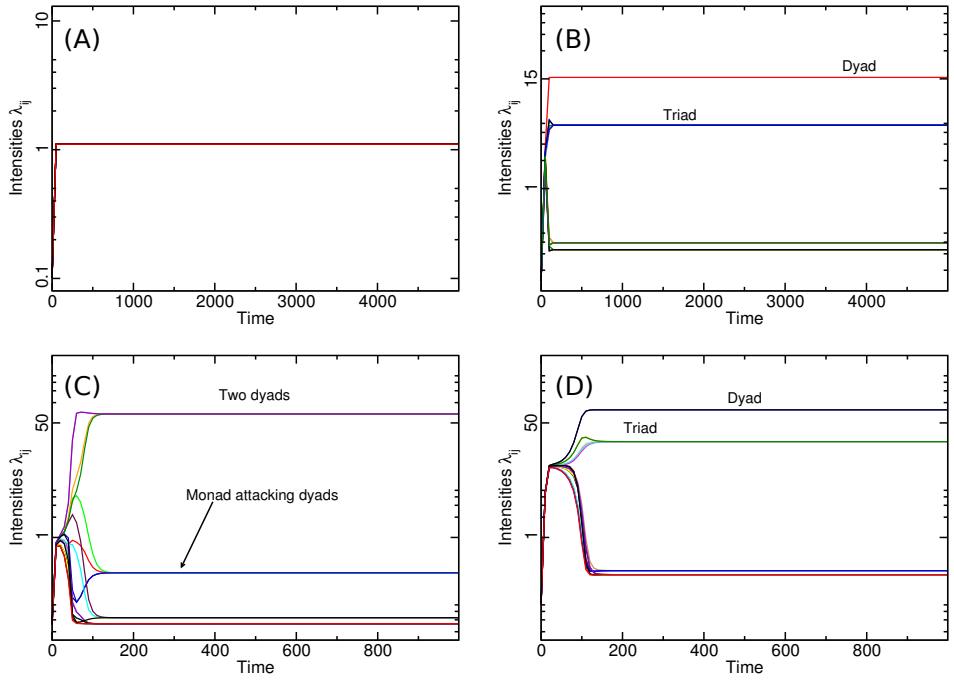

FIGURE 3. Network configurations for $M = 5$ gangs using system (7). The parameters of the various plots (A-D) are equivalent to those used in Fig. 2 above. (A) The homogeneous state $\overline{g}$ with $a = 4$, $b = 1.6$, dimensionless $\mu = 5/1000$. (B) The dyad, triad state with $a = 20$, $b = 8$, dimensionless $\mu = 5/1000$. Unlike the stochastic simulation, the members of the dyad and triad are fixed. (C) The two dyads, monad state with $a = 150$, $b = 5$, dimensionless $\mu = 5/10000$. (D) The dyad, triad state with $a = 10$, $b = 5$, dimensionless $\mu = 1/1000$. In each simulation (A-D), the initial intensity of each rivalry is randomly chosen.

$$\lambda_{3,4} = \left[-2d + q \mp \sqrt{-(4M-9)q^2 - 4(M-3)qu + 4u^2}\right]/2 \ , \tag{11}$$

while the fifth eigenvalue that appears for $M > 3$ is

$$\lambda_5 = -d + q + u \ ; \tag{12}$$

here we have defined

$$d = 1 + [b + a(M-2)]\,(\overline{g} + \mu) > 0, \tag{13}$$

$$u = b(1 - \overline{g} - \mu) > 0, \tag{14}$$

$$q = a\overline{g} > 0 \ . \tag{15}$$

Upon inspection, we can clearly see that $\lambda_1 < 0$. It is also easily shown that $\lambda_2 < 0$ and the real part of $\lambda_3 < 0$. But, it is possible for λ_4 to be real and positive, or for λ_5 to be positive. Specifically, λ_4 will be real and positive if

$$(u+q)\,[u - (M-2)q] > d(d-q) \ , \tag{16}$$

and λ_5 will be positive if

$$u + q > d \ . \tag{17}$$

Note that $\lambda_4 \leq -d+u+q/2 = \lambda_5 - q/2$, so that $\lambda_4 \leq \lambda_5$. Therefore, for $M > 3$ we only concern ourselves with the value of λ_5, as it carries all information about the stability status of the $\overline{g}$ state.

Consider now the special case $\mu = 0$. Here, let $\overline{g} = \overline{g}_M$, which greatly simplifies to

$$\overline{g}_M = \frac{b-1}{b+a(M-2)} \ . \tag{18}$$

The homogeneous solution $g_{ij} = 0$ is also possible in this case, and is in fact the only steady state if $b < 1$, since we only consider values of $g_{ij} \geq 0$. The eigenvalues of this zero rivalry state are $-1 \pm b$; it is therefore stable for $b < 1$ and unstable otherwise. The implication is that when $b < 1$, random acts of violence will not evolve into persistent rivalries, while if $b > 1$, gangs will form persistent rivalries given random violent interactions between them. For $b > 1$, we can determine the stability of the nontrivial $\overline{g}_M$ steady state via the condition (16) or (17) above, dependent upon M. For $M = 3$, we find that $\overline{g}_3$ is unstable ($\lambda_4 > 0$) if $a > b(b+1)$, and for $M > 3$, we find that $\overline{g}_M$ is unstable ($\lambda_5 > 0$) if $a > b$. In general, if third party effects outweigh dyadic interaction strengths, then gangs cannot sustain homogeneous rivalries with a large group, and must instead choose a smaller number of rivals on which to focus their violence.

We now consider what other stable steady states might exist in the $\mu = 0$ case, aside from the $\overline{g}_M$ state discussed above (Fig. 4A). Note that any partitioning of M into isolated, homogeneous components of sizes m_l (such that $\sum_l m_l = M$) is a steady state of our system if $b > 1$ (for $b < 1$, the $\overline{g}_{m_l}$ states do not exist for $m_l > 1$). Here, gangs within any component l are tied together by rivalries of strength $\overline{g}_{m_l}$, and individual components are truly isolated in that there are no rivalry ties between them. However, if $a < b$, isolated components are unstable, and the tendency is for a fully connected homogeneous state to form. On the other hand, if $a > b$, then any component of size $m_k > 3$ is internally unstable. Thus, only partitionings of M consisting of triads ($m_l = 3$), dyads ($m_l = 2$), and monads ($m_l = 1$) may potentially be stable. Within the $a > b$ regime, however, monads are always unstable in the presence of triads; the tendency is for the monad and triad to instead form two pairs. In other words, triads and monads cannot both coexist in a stable steady state of this type. The dividing line between stable triads and monads is the curve $a = b(b+1)$, above which we have already determined that triads are internally unstable (since $\overline{g}_3$ is unstable in this regime). But, even if $a > b(b+1)$, monads are still unstable in the presence of other monads, with two monads preferring to join into a dyad. Hence, there can be at most one monad in this state, which will happen only if M is odd.

The cases above are summarized in Fig. 4A. Here, there are four distinct regions. In gray is the region where the only stable state is $g_{ij} = 0$, occurring for $b < 1$. In blue is the region in which only the $\overline{g}_M$ state is stable, occurring when $a < b$ and $b > 1$. In yellow is the region in which any configuration composed of D dyads and T triads, such that $2D + 3T = M$, is a stable steady state, occurring when $b < a < b(b+1)$ and $b > 1$. Finally, in red is the region where only $M/2$ dyads (for M even) or $(M-1)/2$ dyads and one monad are stable, occurring when $a > b(b+1)$ and $b > 1$.

The states described above do not exhaust all of the possible steady states of the system (7), though we conjecture that any steady state other than those above is unstable. For example, in the $M = 3$ case, there is an unstable steady state in

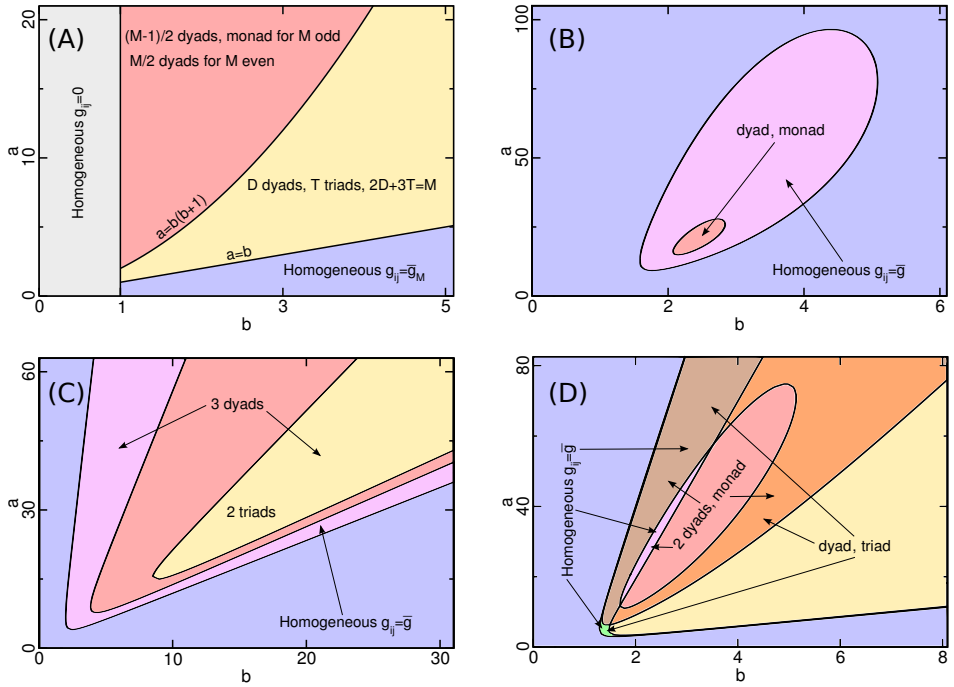

FIGURE 4. Stability diagrams for the system (7). Here, the specific steady states indicated are stable in the region where their label appears as well as where their arrows point. (A) In the $\mu = 0$ case, very general statements can be made about classes of steady state solutions and where they are stable. For $\mu > 0$, there are some general features that depend upon whether M is odd (D), even (C), or the special case $M = 3$ (B). Specifically, we show here (B) $M = 3$, $\mu = 5/1000$; (C) $M = 6$, $\mu = 7/1000$; and (D) $M = 5$, $\mu = 5/1000$.

which two of the gangs have no rivalry strength, but both are heavily attacking the third gang, who attacks each back at a relatively weak rate due to the inhibitory nature of the process. And for higher M values, we have never observed any other steady states of the system in dynamical simulations. In contrast to the stable states described above, all of these presumed unstable steady states will contain some number of asymmetric rivalries, as well as pairs of gangs with no rivalry strength but that share a common rival; we believe these factors contribute to their instability.

For $\mu > 0$, general analytic statements about the stable steady states of the system (7) become more difficult to make. From numerical simulations, however, we observe that the possible stable steady states for $\mu > 0$ are qualitatively similar to those in the $\mu = 0$ case discussed above (Fig. 4). One fundamental difference in the $\mu > 0$ regime, though, is that the major components of the rivalry network – monad, dyads, and triads – are no longer completely isolated, as the rivalry strength between these components must be of at least strength μ. Furthermore, as μ increases, the various non-homogeneous steady states lose stability and/or cease to exist completely. The general trend in this regard is for the system to favor dyads

over triads and triads over the monad, so that the last remaining inhomogeneous steady states appear to be the $M/2$ dyads state for M even; the $(M-3)/2$ dyads, triad state for $M > 3$ and odd; and the dyad, monad state for $M = 3$.

By focusing again on the homogeneous state $\overline{g}$, some of this behavior may be further explained. We first show that there exists a threshold μ_s above which the $\overline{g}$ state for a given M is stable regardless of the values of a and b. For $M = 2$ we clearly have $\mu_s = 0$, since $\overline{g}$ is in fact the only steady state available in this case. For $M > 2$, we find μ_s by setting λ_4 (for $M = 3$) or λ_5 (for $M > 3$) equal to zero, then solving for $\mu(a, b)$. The resulting expression is then maximized simultaneously over b and a to determine the largest value of μ for which $\overline{g}$ may be unstable; i.e., to find μ_s. In the case $M = 3$, the expression is maximized numerically, yielding a value $\mu_s \simeq 0.00515$ when $(b, a) \simeq (2.366, 19.026)$. For $M > 3$, the expression is maximized for $a = b(2M-3)/(M-2)$ and as $b \to \infty$, yielding

$$\mu_s = \frac{1}{(2M-3)^2}. \tag{19}$$

Similarly, there exists a critical value μ_c above which the $\overline{g}$ state is the *only* stable steady state for the system. For $M = 2$ we again trivially have $\mu_c = 0$. For M greater than this, μ_c is found by determining when, as μ increases, the last remaining inhomogeneous steady state ceases to exist. For $M = 3$, this is the dyad, monad state, which we find numerically to cease to exist at $\mu_c \simeq 0.00693$. For $M \geq 4$ and even, the final state is the $M/2$ dyads state, which ceases to exist at

$$\mu_c = \frac{\sqrt{(M-2)(5M-14)^3} - 11M^2 + 56M - 68}{2(M-2)(M-6)^2}. \tag{20}$$

For odd values of $M \geq 5$, the final state is the $(M-3)/2$ dyads, triad state. Unfortunately, we have not yet been able to obtain a general form for μ_c in this case.

In Fig. 4B, we plot the stability diagram for the system using $M = 3$ and $\mu = 5/1000$, which is near μ_s for this case. Here we see that the $\overline{g}$ state is the only stable steady state in the bulk of parameter space (blue). The exceptions are the red region, in which the dyad, monad state is the only stable state, and the purple region, in which both the dyad, monad and $\overline{g}$ states are stable. Note that no such purple region exists when $\mu = 0$. As μ increases, the red and purple regions shrink, disappearing at $\mu = \mu_s$ and $\mu = \mu_c$, respectively.

In Fig. 4C, we plot the stability diagram for the system using $M = 6$ and $\mu = 7/1000$, which is qualitatively representative of all even values $M \geq 4$ that we have observed. Here we find that the stability region for the $M/2$ dyads (red) state has again developed an overlap (shown in purple) with the stability region of the $\overline{g}$ state (blue) as happened in the $M = 3$ case. Moreover, the three dyads region now completely envelops the stability regions of all other D dyad, T triad states (yellow). As μ increases, the nearly straight lines that define the upper and lower bounds of these various regions move toward each other, with the point of intersection of these lines moving to larger values of (b, a). As $\mu \to \mu_c$, regions corresponding to differing D dyad, T triad states disappear, with the red region disappearing next-to-last when $\mu = \mu_s$, and the purple region disappearing last when $\mu = \mu_c$.

Finally, in Fig. 4D, we plot the stability diagram for the system using $M = 5$ and $\mu = 5/1000$, representative of all odd values $M \geq 5$ that we have observed. We see in this case that the region in which the two dyads, monad state has exclusive

stability (red) has become completely surrounded by other regions, existing within a "hole" in the stability region for the dyad, triad state. Furthermore, the stability region of each state now overlaps with those of others. Specifically, the two dyads, monad state overlaps (shown in orange) with the dyad, triad state; the two dyads, monad state overlaps (shown in purple) with the $\overline{g}$ state; the dyad, triad state overlaps (shown in green) with the $\overline{g}$ state; and all three overlap in some regions (shown in brown). As μ increases, the hole in the dyad, triad region begins to close and eventually disappears, destroying the red region. At the same time, the lines defining the upper and lower boundaries of the other regions move closer together as in the $M = 6$ case above, but in such a way that the orange region eventually disappears, leaving only blue, yellow, green, and brown. Next to disappear is brown, when the 2 dyads, monad state has lost stability/existence everywhere. Then, at $\mu = \mu_s$, the yellow region disappears, with only blue and green remaining. The green region is the last to disappear, when $\mu = \mu_c$.

In summary, as the baseline rivalry intensity μ increases, the system of gangs loses the ability to support monads and all but one triad (if M is odd), with all other rivalries being dyadic. If the baseline rivalry intensity is high enough, then the rivalry network resolves to a complete graph with the average rate of violence equally distributed among all possible gang pairs.

5. **Implications for policing strategies.** Reducing gang violence is a high priority in many police departments in large cities, and proactive methods include directed patrols and gang injunctions [17]. Research has shown that deterrence and suppression strategies that focus on a rivalry dyad can significantly reduce violence in the area of intervention without crime displacement to neighboring gangs and geographic regions [25, 32].

The point process model introduced in Section 2 offers a platform on which policing strategies can be tested and optimized for reducing overall violence. This could be useful, as a number of possibilities exist for pre-intervention and post-intervention network configurations corresponding to a particular strategy. For example, if the original network has an even number of gangs, all divided into dyads, and one were to suppress a single dyad, the others dyads will likely remain and the total crime will decrease. However, if the original network has an even number of gangs and includes some number of triads, it is possible that removing a dyad reconfigures the network so that the triads are no longer stable, resulting in an overall increase in crime. For such a system, policing strategies may need to be dynamic in order to reduce the total violence [18].

To illustrate this point further, we consider a system of $M = 7$ gangs, initially characterized by one rivalry triad and two rivalry dyads. We first investigate a policing strategy characterized by focusing all attention on gang 7, the gang with the highest intensity of crime at the time of intervention and a member of one of the dyads. We assume that through directed patrols or injunctions, all crime can be suppressed associated with this gang; i.e., $\lambda_{7k} = 0$ for all rivals k. In Fig. 5A we plot the results of such a strategy. At time step 300 the directed patrols begin and initially the overall rate of crime is reduced (Fig. 5B). However, gang 7's previous rival, gang 6, now disrupts the triad, leading to the formation of a three dyads network, which actually has a higher total rate of crime compared to the original network of seven gangs. Thus, this type of policing strategy actually leads to *more* crime. A more dynamic strategy is displayed in Fig. 5C, where directed patrols switch their focus every seven time steps to whichever gang currently is associated

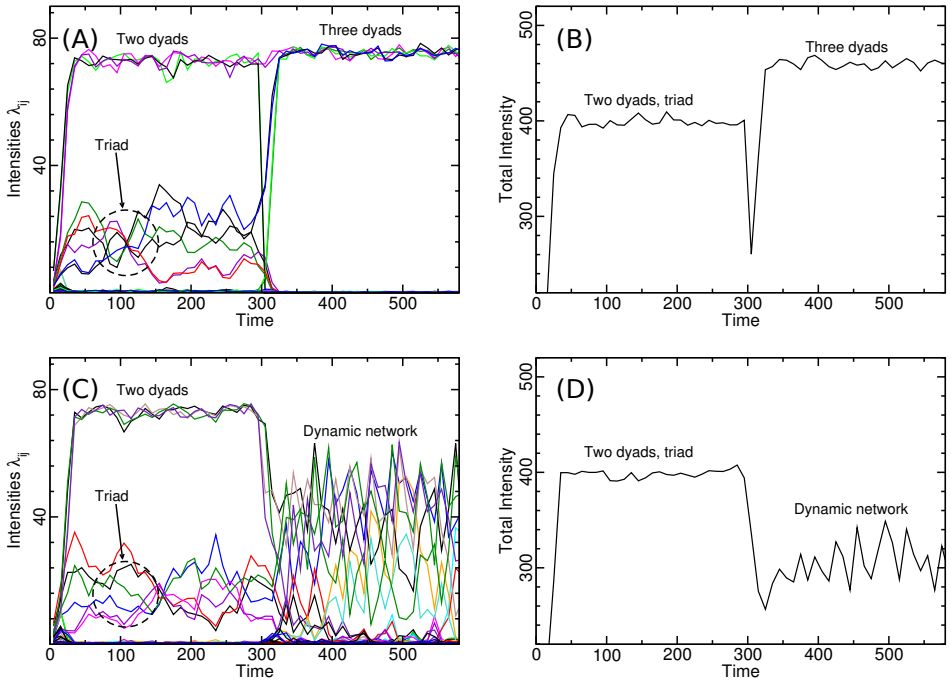

FIGURE 5. Police intervention strategies for an $M = 7$ gang network. (A and B) A static policing strategy, where police enjoin the most violent gang at $t = 300$. (A) Before the injunction, the two dyads, triad state was displayed; after the injunction the effective $M = 6$ network adopts the three dyads state. (B) The total rivalry intensity of the network is higher in the three dyads state, after the injunction. (C and D) A dynamic policing strategy, where police enjoin a new gang every seven time steps starting at $t = 300$. (C) After the injunction, the network behaves dynamically, as new gangs are enjoined quite frequently. (D) After the injunctions begin, the total intensity decreases. Parameter values in both cases are $\mu = 0.2$, $\omega = 0.1$, $\chi = 0.02$, $\theta = 0.5$, $\nu = 0.01$.

with the highest intensity. The result is that all rivalries become transient and the overall rate of crime is reduced (Fig. 5D). It should be noted that the more frequently police switch their focus, the greater the reduction in the overall crime rate.

6. **Hollenbeck gang rivalries.** In this section we focus on 33 gangs residing in or near the 5km by 3km district of Hollenbeck in Los Angeles. Some of the rivalries date back decades, while others are more transient in nature. This complex rivalry network has been examined in [6, 28, 10], and the degree of each node of the network ranges from a few to over 10 rivalry connections, where links can be defined either through interviews of gang members and police officers or through violent crime data where the suspect and victim gang are known (we use the latter in the analysis that follows).

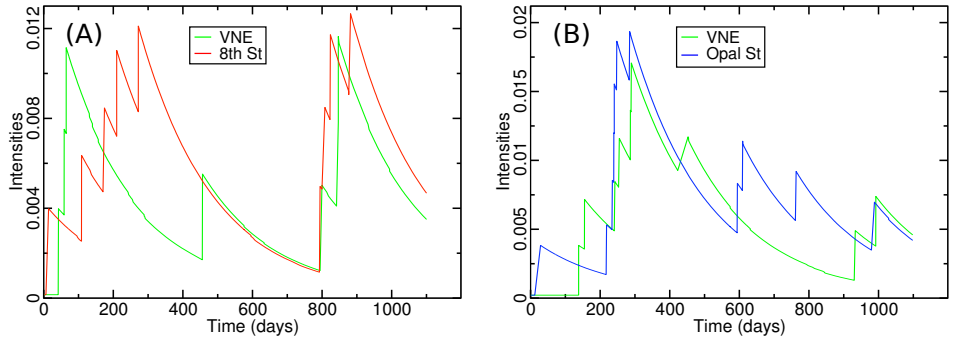

FIGURE 6. Fitted intensities for (A) VNE and 8th Street rivalry and (B) VNE and Opal Street rivalry.

Here we use system (6) to investigate the stability of gang rivalries in Hollenbeck over the time period 1999 to 2002. The data set we consider consists of 349 Part I violent crimes (aggravated assault, homicide, and robbery) committed over a 1044 day span between 1999 and 2002, with each event initiated by one of 33 gangs in Hollenbeck against another one of the 33 gangs. Each event includes the time (in days past the start of the time window), geocoded spatial location, suspected gang, and victim gang (in this study we ignore the spatial information).

We fit system (6) using Maximum Likelihood Estimation (MLE) to the 33 gang network, where the log-likelihood function [4] is given by

$$(\hat{\mu},\hat{\omega},\hat{\chi},\hat{\theta},\hat{\nu}) = \underset{(\mu,\omega,\chi,\theta,\nu)}{\operatorname{argmax}} \left\{ \sum_{i\neq j} \left(\sum_{n=1}^{N_{ij}(T)} \log\left(\lambda_{ij}(t_{ij-}^{n})\right) - \int_0^T \lambda_{ij}(t)dt \right) \right\}, \quad (21)$$

and T is the time interval of observations (1044 days in our case). The first term in the log-likelihood function leads to the selection of parameter values for which more probability mass is placed at the event times and the second term forces the intensity to (approximately) integrate to the total number of events in the data set. The negative log-likelihood function is minimized using the built in Matlab routine "fminsearch", and we use the homogeneous initial condition $\lambda_{ij}(0) = \mu$ for the starting value of each rivalry intensity.

MLE yields the parameter estimates $\hat{\mu} = .000124$, $\hat{\omega} = .00491$, $\hat{\chi} = .0164$, $\hat{\theta} = .00356$, and $\hat{\nu} = .0193$, which fall into the homogeneous region of parameter space. The baseline rate μ corresponds to an approximate rate of 1 event per 10,000 days, thus an unprovoked attack between any rivalry pair is a relatively rare event. However, the intensity increases by a factor of (approx.) 30 after an initial attack, leading to the formation of transient hotspots in the rivalry network. There is also a significant inhibitory effect through the rivalry network due to occurrence of an attack, reflected in the estimate of χ. We plot an example of a fitted subnetwork in Fig. 6 that illustrates the coupling of rivalry intensities among gangs VNE, Opal St., and 8th St.

One method for validating the model consists of constructing a baseline model for comparison and then using a model selection criterion, such as the Akaike Information Criterion (AIC) [16], to compare the competing models. The AIC favors models with higher likelihood value, but penalizes over-parameterization. A lower AIC value indicates the favored model.

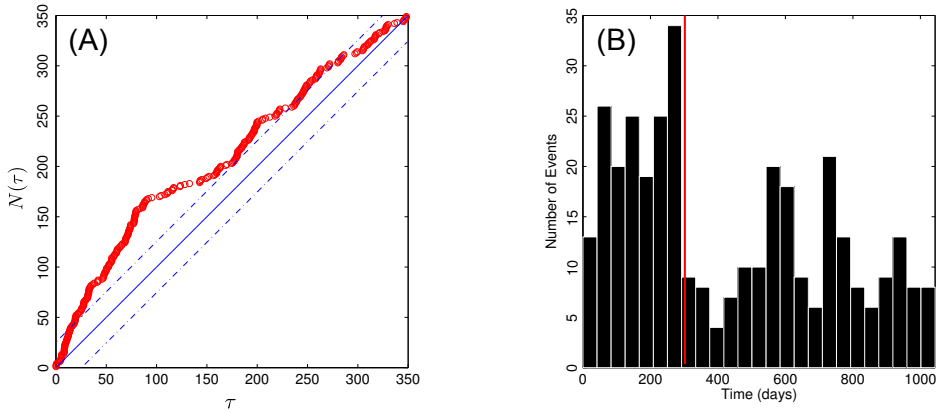

FIGURE 7. (A) Full 33 gang network cumulative number of events $N(\tau)$ vs. rescaled event times τ (red circles), along with the average (solid blue) value for a unit rate Poisson process and 95% error bounds (dashed blue) for the Kolmogorov-Smirnov statistic. Right: Histogram of event count by day and proposed change point in background rate μ (red line), chosen due to the apparent drop in activity after that time.

A stationary Poisson process serves as a possible baseline model in this case. Consider the weighted, directed adjacency matrix A, with entry A_{ij} corresponding to the number of attacks by gang i on gang j. The MLE rate for each directed rivalry for the stationary Poisson process is then $\lambda_{ij}^{\text{poisson}} = A_{ij}/T$. We find that the AIC values for system (6) and the Poisson process are $5,338$ and $6,499$, respectively, and thus the point process model (6) is favored.

Alternatively, residual analysis can be used to assess the goodness of fit without respect to a competing model. For example, the rescaled event times,

$$\tau^n = \int_0^{t^n} \sum_{i \neq j} \lambda_{ij}(t) dt, \tag{22}$$

should follow a unit rate Poisson process if the model is correctly specified [21]. In Fig. 7, we plot the cumulative number of events $N(\tau)$ vs. the rescaled event times τ for the MLE version of (6) described above. We note that the estimated intensity significantly underestimates the actual rate of events in the first 300 days of the data, leading to many more events occurring than the model would predict, such that the model can be rejected in this form.

One possible explanation for the lack of fit is that the background rate μ is not stationary, but instead is influenced by exogenous events [16]. We next re-estimate the model under the assumption that a change point occurred in the background rate, as depicted in Fig. 7. We denote the background rate before and after the change point as μ_1 and μ_2, respectively.

To better fit the data, we also remove 7 gangs from the network that were each involved in 2 or less crimes throughout the three year period, as their inclusion biases parameter estimates in the network. While one possibility for rivalry inactivity between two gangs is the absence of background events triggered at a low rate μ, another possibility is that the gangs are not connected in the network (i.e., $\mu = 0$) and thus the overall network is a collection of disjoint subnetworks. We

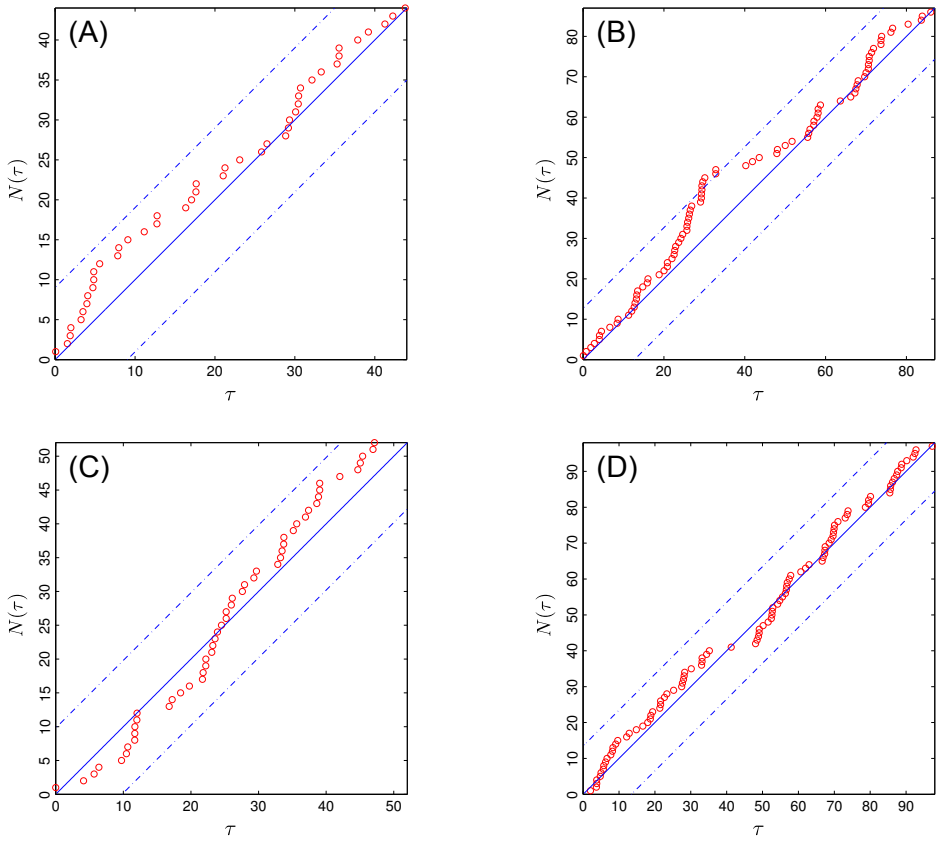

FIGURE 8. Cumulative number of events $N(\tau)$ vs. rescaled event times τ (red circles), along with the average (solid blue) value for a unit rate Poisson process and 95% error bounds (dashed blue) for the Kolmogorov-Smirnov statistic, plotted for each of the gang subnetworks: (A) subnetwork I with M=4, (B) subnetwork II with M=8, (C) subnetwork III with M=5, and (D) subnetwork IV with M=9. In the case of subnetwork II, the data does slightly exit the 95% bound, but is well within the 98% bound, making this a borderline case.

therefore partition the remaining 26 gang network into subnetworks of rival gangs by applying the partitioning algorithm detailed in [11] to $(A + A^{\mathrm{T}})/2$, with A the directed adjacency matrix described above.

We estimate the model parameters for each subnetwork using Metropolis Hastings [27] with a normal proposal transition density and uninformative exponential priors, exp(.01), over the model parameters μ_1, μ_2, ω, and θ. We use a uniform prior for χ, as this parameter is restricted to the range $[0, 1]$. We take the prior distribution of ν to be exp(1), as the model suffers from a parameter identifiability issue (in the continuum limit there are three effective parameters). Convergence is assessed by visual inspection of the trace plots of the sampled posterior distributions.

In Fig. 8, we plot the cumulative number of events $N(\tau)$ vs. the rescaled event times τ for the fitted intensities of each of the subnetworks. Model parameters are estimated from the posterior mean. For three out of the four subnetworks, the

TABLE 1. Estimated Parameters

subnetwork	I ($M = 4$)	II ($M = 8$)	III ($M = 5$)	IV ($M = 9$)
μ_1	.0035 (.0012)	.0011 (.0003)	.0032 (.0010)	.0009 (.0002)
μ_2	.0011 (.0004)	.0005 (.0001)	.0009 (.0004)	.00017 (.00007)
χ	.17 (.15)	.16 (.11)	.12 (.16)	.092 (.067)
ν	.98 (.89)	1.05 (1.06)	.98 (.84)	1.08 (.95)
ω	.020 (.009)	.008 (.003)	.011 (.014)	.005 (.001)
θ	.011 (.005)	.005 (.002)	.004 (.003)	.005 (.001)
$\tilde{\mu}_1$	.0034	.0012	.0032	.00097
$\tilde{\mu}_2$	.0011	.0005	.0009	.00019
a	8.5	18.9	11.6	16.8
b	.56	.68	.35	.95

cumulative distribution stays within the 95% bounds for a unit rate Poisson process (the other subnetwork is still well within the 98% bound, making it a borderline case), and in general we find the model to yield a good fit to the data in comparison to a stationary Poisson process: the AIC for system (6) in this case is 3711.1, while a stationary Poisson on these subnetworks has an AIC of 3899.4.

In Table 1, we list the posterior mean and standard deviations of the parameters for the four subnetworks. Across all of the sub-networks excitation is detected. The estimated values for θ indicate that the rivalry intensities increase by up to a factor of 5 over baseline rates following the occurrence of an event. The gangs in each of the sub-networks also display inhibition following a crime, reflected in the estimated values of χ, though we note that there is high uncertainty in these parameter estimates. In fact, a large portion of our estimated parameters have significant standard deviation compared to the mean, making any specific conclusions as to the actual values of these parameters difficult. However, though the exact parameters are not well established from our (relatively sparse) dataset, Fig. 8 still reflects that the model fits the data well.

For each sub-network, the non-dimensionalized parameters again fall into the homogeneous region of the stability diagram. Thus, it seems appropriate to classify each sub-network as fundamentally a complete graph with equal rivalry ties proportional to $\overline{\lambda}_M$. Elevated rivalries may form for intermediate time periods, but they are likely to be replaced by new rivalries with equal probability. These results indicate that crime hotspots in Hollenbeck may be produced by stochastic fluctuations, rather than by static differences in rivalry relations.

7. **Conclusion.** We developed a point process model for the simulation of gang rivalry networks, paying close attention to the network dynamics that emerge due to excitation and inhibition. The model is capable of reproducing hotspots similar to those observed in gang violence data and is amenable to fast simulation and parameter estimation. We investigated the dependence of network configurations on the model parameters and derived conditions for which homogeneous rivalry networks occur, akin to a complete graph. We illustrated how the model can be used to test policing strategies before they are implemented in the field. This could be important since the complex, nonlinear network of gang rivalries may respond in counter-intuitive ways to a given strategy. By fitting the model to gang violence

data, we explored the levels of excitation, inhibition, and the stability of gang rivalries in Hollenbeck, Los Angeles.

Acknowledgments. The authors would like to thank Tawny Lim and Anthony DeCino for helpful discussions and the LAPD for providing the data used in this study.

REFERENCES

[1] E. Anderson, *Code of the Street: Decency, Violence, and the Moral Life of the Inner City*, Norton, New York, 1999.
[2] C. Boehm, *Blood Revenge: The Anthropology of Feuding in Montenegro and Other Tribal Societies*, University of Pennsylvania Press, Philadelphia, 1987.
[3] M. Cooney, *Warriors and Peacemakers: How Third Parties Shape Violence*, New York University Press, New York, 1998.
[4] D. Daley and D. Vere-Jones, *An Introduction to the Theory of Point Processes*, 2^{nd} edition, Springer, New York, 2008.
[5] S. H. Decker and G. D. Curry, Gangs, gang homicides, and gang loyalty: Organized crimes or disorganized criminals, *Journal of Criminal Justice*, **30** (2002), 343–352.
[6] M. Egesdal, C. Fathauer, K. Louie and J. Neuman, Statistical and stochastic modeling of gang rivalries in Los Angeles, *SIURO*, **3** (2010), 72–94.
[7] J. Fagan, The social organization of drug use and drug dealing among urbang gangs, *Criminology*, **27** (1989), 633–670.
[8] G. Farrell and K. Pease (eds.), *Repeat Victimization*, Criminal Justice Press, New York, 2001.
[9] M. R. Gottfredson and T. Hirshi, *A General Theory of Crime*, Stanford University Press, 1990.
[10] R. A. Hegemann, L. M. Smith, A. Barbaro, A. L. Bertozzi, S. Reid and G. E. Tita, Geographical influences of an emerging network of gang rivalries, *Physica A*, **390** (2011), 3894–3914.
[11] J. Hespanha, *An efficient MATLAB Algorithm for Graph Partitioning*, Technical report, 2004. Available from: `http://www.ece.ucsb.edu/~hespanha/techrep.html`.
[12] B. A. Jacobs and R. Wright, *Street Justice: Retaliation in the Criminal Underworld*, Cambridge University Press, Cambridge, 2006.
[13] S. D. Johnson, Repeat burglary victimisation: A tale of two theories, *Journal of Experimental Criminology*, **4** (2008), 215–240.
[14] P. Jones, P. J. Brantingham and L. Chayes, Statistical models of criminal behavior: The effects of law enforcement actions, *M3AS*, **20** (2010), 1397–1423.
[15] M. W. Klein and C. L. Maxson, *Street Gang Patterns and Policies*, Oxford University Press, New York, 2006.
[16] E. Lewis, G. O. Mohler, P. J. Brantingham and A. Bertozzi, Self-exciting point process models of civilian deaths in Iraq, *Security Journal*, **25** (2011), 244–264.
[17] C. Maxson, Street gangs, in *Crime and Public Policy* (eds. J. Q. Wilson and J. Petersilia), Oxford University Press, New York, (2011), 158–182.
[18] G. O. Mohler, M. B. Short, P. J. Brantingham, F. Schoenberg and G. E. Tita, Self-exciting point process modeling of crime, *Journal of the American Statistical Association*, **106** (2011), 100–108.
[19] Y. Ogata, Space-time point process models for earthquake occurrences, *Ann. Inst. Statist. Math.*, **50** (1998), 379–402.
[20] Y. Ogata, On lewis' simulation method for point processes, *IEEE*, **27** (1981), 23–31.
[21] Y. Ogata, Statistical models for earthquake occurrences and residual analysis for point processes, *Journal of American Statistical Association*, **83** (1988), 9–27.
[22] A. V. Papachristos, *Murder by Structure: A Network Theory of Gang Homicide*, Ph.D thesis, University of Chicago, 2007.
[23] A. V. Papachristos, Murder by structure: Dominance relations and the social structure of gang homicide, *American Journal of Sociology*, **115** (2009), 74–128.
[24] S. Phillips and M. Cooney, Aiding peace, abetting violence: Third parties and the management of conflict, *American Sociological Review*, **70** (2005), 334–354.
[25] A. M. Piehl, D. M. Kennedy and A. A. Braga, Problem solving and youth violence: An evaluation of the Boston Gun Project, *American Law and Economics Review*, **2** (2000), 58–106.

[26] A. B. Pitcher, Adding police to a mathematical model of burglary, *European Journal of Applied Mathematics*, **21** (2010), 401–419.
[27] S. Ross, *Simulation*, Second edition. Statistical Modeling and Decision Science. Academic Press, Inc., San Diego, CA, 1997.
[28] S. M. Radil, C. Flint and G. E. Tita, Spatializing social networks: Using social network analysis to investigate geographies of gang rivalry, territoriality and violence in Los Angeles, *Annals of the Association of American Geographers*, **100** (2010), 307–326.
[29] N. Rodriguez and A. L. Bertozzi, Local existence and uniqueness of solutions to a PDE model for criminal behavior, *M3AS*, **20** (2010), 1425–1457.
[30] T. A. Taniguchi, J. H. Ratcliffe and R. B. Taylor, Gang set space, drug markets, and drime around drug corners in Camden, *Journal of Research in Crime and Delinquency*, **48** (2011), 327–363.
[31] G. E. Tita and G. Ridgeway, The impact of gang formation on local patterns of crime, *Journal of Research in Crime and Delinquency*, **44** (2007), 208–237.
[32] G. E. Tita, J. K. Riley, G. Ridgeway, C. Grammich, A. F. Abrahamse and P. Greenwood, *Reducing Gun Violence: Results from and Intervention in East Los Angeles*, RAND Press, Santa Monica, 2003.
[33] M. B. Short, M. R. D'Orsogna, V. Pasour, G. E. Tita, P. J. Brantingham, A. L. Bertozzi and L. Chayes, A statistical model of criminal behavior, *M3AS*, **18** (2008), 1249–1267.
[34] M. B. Short, P. J. Brantingham, A. L. Bertozzi and G. E. Tita, Dissipation and displacement of hotspots in reaction-diffusion models of crime, *PNAS*, **107** (2010), 3961–3965.
[35] M. B. Short, M. R. D'Orsogna, P. J. Brantingham and G. E. Tita, Measuring and modeling repeat and near-repeat burglary effects, *J. Quant. Criminol.*, **25** (2009), 325–339.

Received March 2011; revised June 2012.

E-mail address: mbshort@math.gatech.edu
E-mail address: gmohler@scu.edu
E-mail address: pjb@anthro.ucla.edu
E-mail address: gtita@uci.edu